OPEN ACCESS

Energy Conversion ARTICLE

The Innovation Energy

Experimental study on multi-mode start-up and dynamic characteristics of proton exchange membrane (PEM) electrolyzer system

Hao Zhang,[1] Pengyun Wang,[1] Lin Zhao,[1] Qibin Li,[1,*] Haoshui Yu,[2] Tao Yang,[3,*] and Jun Shen[3]

*Correspondence: qibinli@cqu.edu.cn(Q. L.); yangtao@bit.edu.cn(Y. T.)

Received: February 6, 2026; Accepted: April 14, 2026; Published Online: April 22, 2026; https://doi.org/10.59717/j.xinn-energy.2026.100160

GRAPHICAL ABSTRACT

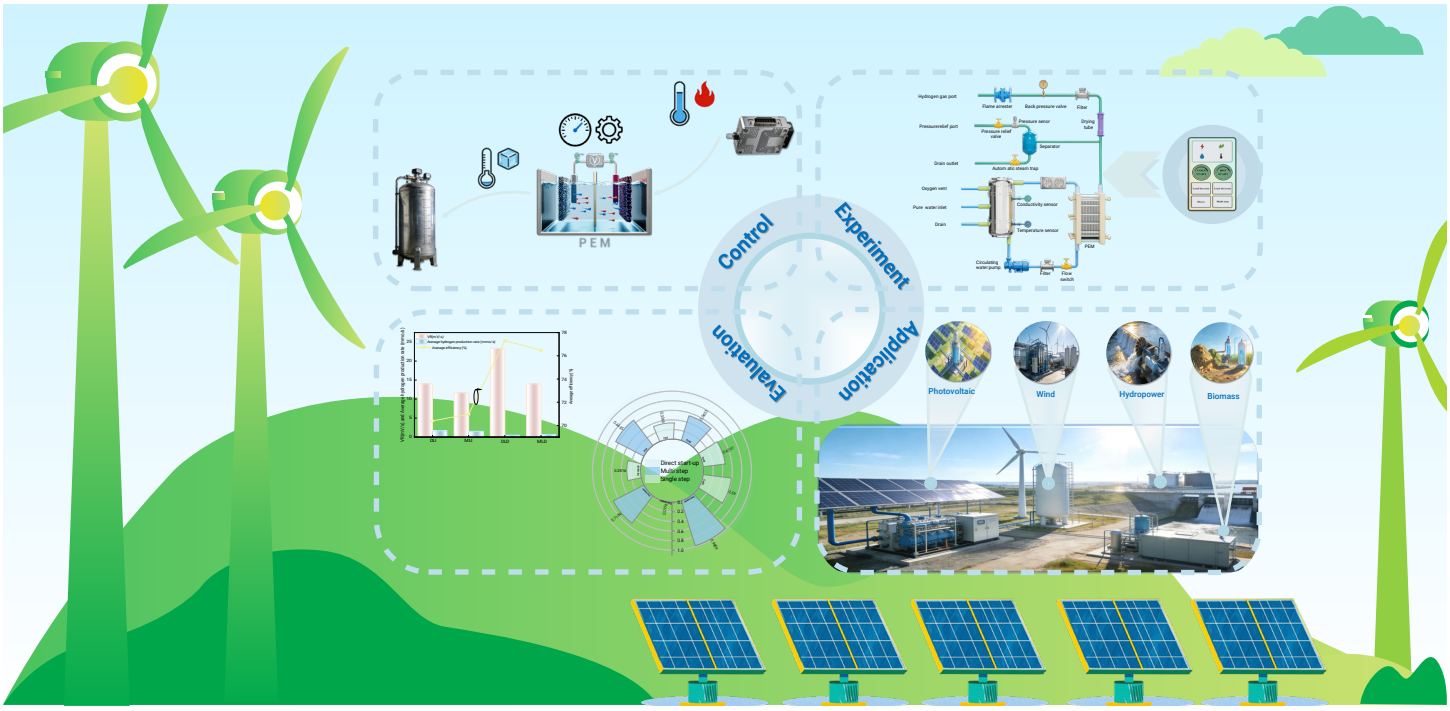

PUBLIC SUMMARY

- Systematic experimental investigation of PEM electrolyzer dynamics covering cold start, hot start, and load regulation.
- An entropy-TOPSIS integrated evaluation framework for objective and quantitative dynamic performance assessment.
- Identification of critical current threshold enabling effective hot start-up to inform rapid operational strategies.
- Stepwise load regulation proves superior in enhancing system efficiency and stability, especially during unloading.

ARTICLE Energy Conversion

www.the-innovation.org/the-innovation-energy

Experimental study on multi-mode start-up and dynamic characteristics of proton exchange membrane (PEM) electrolyzer system

Hao Zhang,[1] Pengyun Wang,[1] Lin Zhao,[1] Qibin Li,[1,*] Haoshui Yu,[2] Tao Yang,[3,*] and Jun Shen[3]

[1]Key Laboratory of Low-grade Energy Utilization Technologies & Systems, Ministry of Education, School of Energy and Power Engineering, Chongqing University, Chongqing 400044, China

[2]Department of Chemistry and Bioscience, Aalborg University, Niels Bohrs Vej 8A, Denmark

[3]School of Mechanical Engineering, Beijing Institute of Technology, Beijing 100081, China

*Correspondence: qibinli@cqu.edu.cn(Q. L.); yangtao@bit.edu.cn(Y. T.)

Received: February 6, 2026; Accepted: April 14, 2026; Published Online: April 22, 2026; https://doi.org/10.59717/j.xinn-energy.2026.100160

Citation: Zhang H., Wang P., Zhao L., et al. (2026). Experimental study on multi-mode start-up and dynamic characteristics of proton exchange membrane (PEM) electrolyzer system. *The Innovation Energy* **3**:100160.

This study experimentally investigates and comparatively analyzes the dynamic performance of a proton exchange membrane (PEM) electrolyzer during cold start, hot start, and load regulation. The experimental comparison specifically includes three cold start-up strategies: direct, single-step, and double-step; two hot start-up approaches: direct and multi-step; and two load regulation modes: direct and stepwise. To comprehensively evaluate the dynamic performance of the PEM electrolyzer, this study adopts indicators such as voltage rise rate, average efficiency, and average hydrogen production rate for assessment. To objectively determine the weights of each indicator, the entropy weight method was adopted. Subsequently, the Technique for Order Preference by Similarity to Ideal Solution (TOPSIS) was used to calculate the closeness coefficient of each operational strategy to the ideal solution, thereby quantifying their overall performance ranking. Results show that the single-step cold start-up strategy exhibits the best overall performance, with its voltage rise rate, average efficiency, and average hydrogen production rate being 2.32 mV/s, 69.68%, and 1.324 mmol/s, respectively. The multi-step hot start-up strategy demonstrates superior overall performance compared to the direct hot start-up, with corresponding indicators of 4.25 mV/s, 71.92%, and 1.315 mmol/s, respectively. The multi-step load regulation strategy exhibits significantly better overall performance than the direct regulation method, particularly during load-decreasing operations. The relative closeness coefficients are 0.2816 and 0.7184 for direct and multi-step load increasing, respectively, and 0.0196 and 0.9804 for direct and multi-step load decreasing, respectively. This study provides both experimental evidence and a comprehensive assessment framework for optimizing the dynamic operation strategies of PEM electrolyzers.

INTRODUCTION

Given the depletion of fossil fuels and rising greenhouse gas emissions, advancing renewable energy technologies is imperative.[1] The global pursuit of carbon neutrality drives large-scale integration of renewable energy into the grid, yet this presents challenges for grid regulation.[2,3] Integrating energy storage, particularly hydrogen energy storage, offers a pivotal solution by converting surplus electricity into storable hydrogen, providing grid flexibility and security.[4,5] Hydrogen, used via fuel cells or combustion, completes the clean energy cycle with water as the only byproduct,[6] and holds transformative potential across various sectors.[7]

The International Energy Agency estimates that achieving global net zero by 2050 will require around 520 million tons of low-carbon hydrogen, with renewables expected to supply nearly 60% as green hydrogen.[8] However, current global production remains at 75 million tons annually, with 95% derived from fossil fuels.[9] Replacing gray hydrogen with green hydrogen is crucial for decarbonizing the chemical industry,[10] making water electrolysis a key production method.[11]

Water electrolysis is the process of splitting water into hydrogen and oxygen using electrical energy. The primary electrolysis technologies currently include alkaline water electrolysis (AWE), proton exchange membrane electrolysis (PEM), and solid oxide electrolysis cell (SOEC).[12-14] While AWE is mature, its slow dynamic response limits efficient integration with intermittent renewables.[15] SOEC, despite high theoretical efficiency, is constrained by material degradation at high temperatures and a slow start.[16] In contrast, PEM presents a promising solution to these limitations. It exhibits key advantages such as rapid dynamic response, high current density operation, and high-purity hydrogen production, which collectively render it highly suitable for grid integration and consumption of variable renewable energy.[17,18]

Multiple studies have investigated the performance of PEM hydrogen production systems through simulations. Midilli et al.[19] analyzed the influence of operating parameters on a PEM electrolysis system coupled with high-pressure hydrogen storage using exergetic sustainability indicators. Their results revealed that at a storage pressure of 400 bar, increasing the electrolyzer operating pressure from 10 bar to 100 bar improved the system exergy efficiency from 59.8% to 61.5%. Ganjehsarabi et al.[20] optimized a geothermal-driven organic Rankine cycle (ORC) coupled with a PEM system using a working fluid mixture comprising 60% butane and 40% pentane. This configuration achieved a hydrogen yield of 45.57 g/h per unit geothermal flow, with an exergy efficiency of 38.8% and a hydrogen production cost of 85-95 $/kg, primarily attributed to the electrolyzer. For a solar-driven hydrogen production and liquefaction system, Corumlu et al.[21] reported overall energy and exergy efficiencies of 22.97% and 19.55%, respectively. Key findings indicated that higher solar irradiance and electrolyzer temperature enhanced efficiencies, while a 40 °C in ambient temperature improved system exergy efficiency by approximately 30% and increased hydrogen yield. Rauls et al.[22] investigated the start-up behavior of PEM water electrolyzers and proposed heat-up efficiency and a dimensionless heat-up number. They found that a partial-load start-up (1.80 V) achieved the highest heat-up efficiency of 74.0%. However, their study primarily focused on electric heating start-up strategies and did not compare cold and hot start-ups under multi-stage current control. Sakas et al.[23] developed and validated a dynamic, parameter adjustable mass and energy balance model for a 50 kW PEM electrolyzer plant. The model integrated electrochemical, thermal, and mass transfer submodels for the stack and auxiliary components. Validation against industrial data demonstrated high accuracy, with 98.32% for thermal behavior and 98.64% for hydrogen production prediction. Analysis showed that 68.5% of the stack input power was converted to hydrogen under nominal operation, while the remaining 31.5% was dissipated as heat due to overpotentials. Bulut et al.[24] established a mathematical model to optimize hydrogen production in an integrated photovoltaic-proton exchange membrane electrolyzer (PV-PEM) system, examining the effects of operating temperature and membrane thickness. The model was also applied to evaluate regional hydrogen production potential. Optimal performance was achieved at 80 °C with a thinner membrane, yielding a peak hydrogen production rate of 1.82 mL/min. Scaling to multi-cell stacks, maximum production reached about 350 mL/min for 7 cells and 700 mL/min for 14 cells. The overall system efficiencyinfluenced by solar irradianceranged from 6.0% to 6.5%.

Several experimental studies have been published to date. Mraoui et al.[25] conducted experimental and numerical investigations on a directly coupled photovoltaic-proton exchange membrane (PV-PEM) electrolyzer system for hydrogen production. The photovoltaic panel was modeled using a five-parameter model, and an empirical model was applied to the electrolyzer, both achieving a root mean square error (RMSE) of approximately 2%. However, the overall system simulation exhibited a discrepancy with theex-

perimental results, with an RMSE of about 7%, which was primarily attributed to the slower-than-expected dynamic response of the electrolyzer. Keller et al.[26] experimentally validated a dynamic demand response scheduling method that utilizes thermal management to enable short-term overload operation, reducing operating costs by 3.8% over a 6-hour scheduling period. However, their study focused primarily on economic dispatch and lacked a comprehensive evaluation of multiple indicators such as voltage ramp rate, efficiency, and hydrogen production rate during the start-up process. Kesercioglu et al.[27] applied the Taguchi method to optimize the operating temperature, clamping torque, and water flow rate of a PEM electrolyzer, identifying optimal conditions of 80°C, 10 Nm, and 10 mL/min. However, their study primarily focused on steady-state parameter optimization and did not compare dynamic start-up and load regulation strategies. Collectively, these studies provide an important foundation for the dynamic operation of PEM electrolyzes; however, systematic experimental comparisons of different control strategies during cold start, hot start, and load regulation processes, along with research incorporating multi-indicator comprehensive evaluation methods, remain insufficient.

Current research on PEM electrolyzers mostly focuses on steady-state optimization and system integration, while experimental studies on dynamic responses during start-up and under varying conditions are limited. This gap hinders the development of accurate dynamic models and effective control strategies for renewable energy systems. Therefore, this study systematically investigates the real-time response of PEM electrolyzers during different start-ups and dynamic conditions. It also applies the entropy weight method and TOPSIS for performance evaluation, aiming to support model development and control strategies.

MATERIALS AND METHODS

The experimental platform

The experimental platform employs a PEM electrolyzer system, model XRA-WESOOM-A2000ML manufactured by Xingran Technology Co., Ltd., China. The unit features a rated power of 600 W, consisting of eight electrolytic cells connected in series. The system delivers a hydrogen production rate adjustable from 0 to 2000 mL/min, with an output pressure up to 1.5 MPa and hydrogen purity exceeding 99.99%. The system integrates four subsystems: feed water, hydrogen processing, and oxygen venting. The hydrogen processing subsystem handles separation, purification, and solid-state storage. All sensors for temperature, pressure, flow rate, and conductivity are calibrated regularly in accordance with manufacturer standards. Hydrogen flow rate is measured using a mass flow controller. Voltage and current signals are acquired via a high-precision NI DAQ system with an accuracy of ±0.1%. Stack voltage is measured directly at the stack terminals to minimize contact resistance. The system operates under closed-loop automatic control of pressure, temperature, and water level, and is equipped with built-in safety interlocks to detectover-temperature and water quality abnormalities. The experimental schematic diagram is shown in Figure 1A.

The system comprises four main subsystems:

(1) The feed water system, which continuously supplies high-purity water;

(2) The circulation system, which actively removes reaction heat and gases to maintain a stable internal environment;

(3) The hydrogen system, which handles separation, purification, storage (in solid-state cylinders), and delivery;

(4) The oxygen system, which manages separation and venting, typically serves as the reference for monitoring system pressure and temperature.

Standard equipment includes monitoring instruments for temperature, flow rate, and water conductivity, along with gas-liquid separators, a pressure regulation system, safety valves, and gas drying lines. The main technical parameters of the PEM electrolysis system are listed in Figure 1B.

Experimental procedure

The experimental campaign was divided into two phases: the first seven experimental sets were designed to compare the dynamic response characteristics under cold and hot start-up conditions across different control strategies, and the subsequent four sets focused on evaluating the system's performance under various current disturbance tests.

The standard operating procedure for a cold start-up is as follows: First, fill the water tank to the preset level and set the initial temperature of the PEM electrolyzer to 10 °C. Then, start-up the system according to the manufacturer's instructions, and set the target operating current and temperature safety threshold. The electrolyzer possesses an inherent self-heating capability, whereby the heat generated during operation is sufficient to raise its temperature without external heat requirement. Once stable operation is achieved, the system continuously monitors all operational parameters. If water quality abnormalities are detected or the electrolyzer temperature exceeds the set safety threshold, the protection mechanism is triggered immediately, resulting in an automatic system shutdown. The system can only be restarted after the underlying issues have been resolved and all parameters are confirmed to be reset within normal ranges.

To evaluate the effects of different current control strategies on the system cold start-up process and dynamic response characteristics, this study designed and conducted three sets of comparative experiments, encompassing three start-up strategies: the direct cold start-up (DCS) strategy sets the operating current directly to the rated value of 40 A upon system start-up, allowing the electrolyzer to heat up to the rated operating temperature of 40°C under constant load; the single-step cold start-up (SCS) strategy adopts a two-stage current step, starting at 25 A and self-heating until stable at 25°C, then increasing the current to 40 A to drive the system to the target temperature; the multi-step cold start-up (MCS) strategy employs a three-stage current sequence (15 A→30 A→40 A), with each stage corresponding to a specific thermal stabilization temperature point (10°C, 20°C, and 30°C, respectively), requiring the system to reach the current temperature setpoint before advancing to the next current stage.

For the hot start-up experiments, the PEM electrolyzer was preheated to an initial temperature of 30°C prior to each test. Two distinct current control strategies were implemented and compared:

(1) Direct hot start-up (DHS): In this strategy, the operating current was directly stepped from 0 A to the rated value of 40 A upon system start-up. The electrolyzer then self-heated from 30°C to the target operating temperature of 40°C under constant current load. (2) Multi-step hot start-up (MHS): This strategy employed a stepwise current loading profile. The current was sequentially increased from 0 A to 26 A, then to 33 A, and finally to 40 A. Correspondingly, the electrolyzer temperature was required to stabilize progressively at 30°C, 33°C, 36°C, and ultimately reach the target temperature of 40°C at each respective step. Each current step was initiated only after the system had reached thermal equilibrium at the preceding temperature setpoint.

The fundamental difference between cold and hot start-up lies in the fact that the former begins from a lower initial thermal state of the stack. This comparison is systematically presented in Table 1.

Cold start-up simulates system activation after a prolonged shutdown (overnight or during low renewable energy periods). Investigating its dynamic characteristics helps ensure reliable restart and optimizes control strategies to reduce thermal stress and energy consumption during the heating phase. Hot start-up simulates scenarios where the system is briefly idled but remains at elevated temperatures (grid fluctuations or intermittent renewable supply). Under such conditions, fast response capability is critical for grid balancing, and optimizing hot start-up strategies can enhance system flexibility and overall efficiency.

Following the foundational investigation into system start-up characteristics, this study designed and conducted a series of current step change disturbance experiments to further examine the response of the PEM electrolysis system under dynamic operating conditions. The experimental framework encompasses two typical disturbance modes: current increase and current decrease. Two distinct test sequences with different pathways were designed for each mode, resulting in a total of four comparative experimental sets. The specific current disturbance profiles implemented include: a single-step positive step change from 25 A to 40 A; a progressive load increase from 25 A through 30 A and 35 A to 40 A; a single-step negative step change from 25 A to 10 A; and a progressive load decrease from 25 A through 20 A and 15 A to 10 A. The experiments aimed to evaluate the impact of different current variation patterns on the operational performance of the PEM electrolysis system. To this end, the dynamic evolution of key system parameters was monitored within defined time windows after each distur-

A

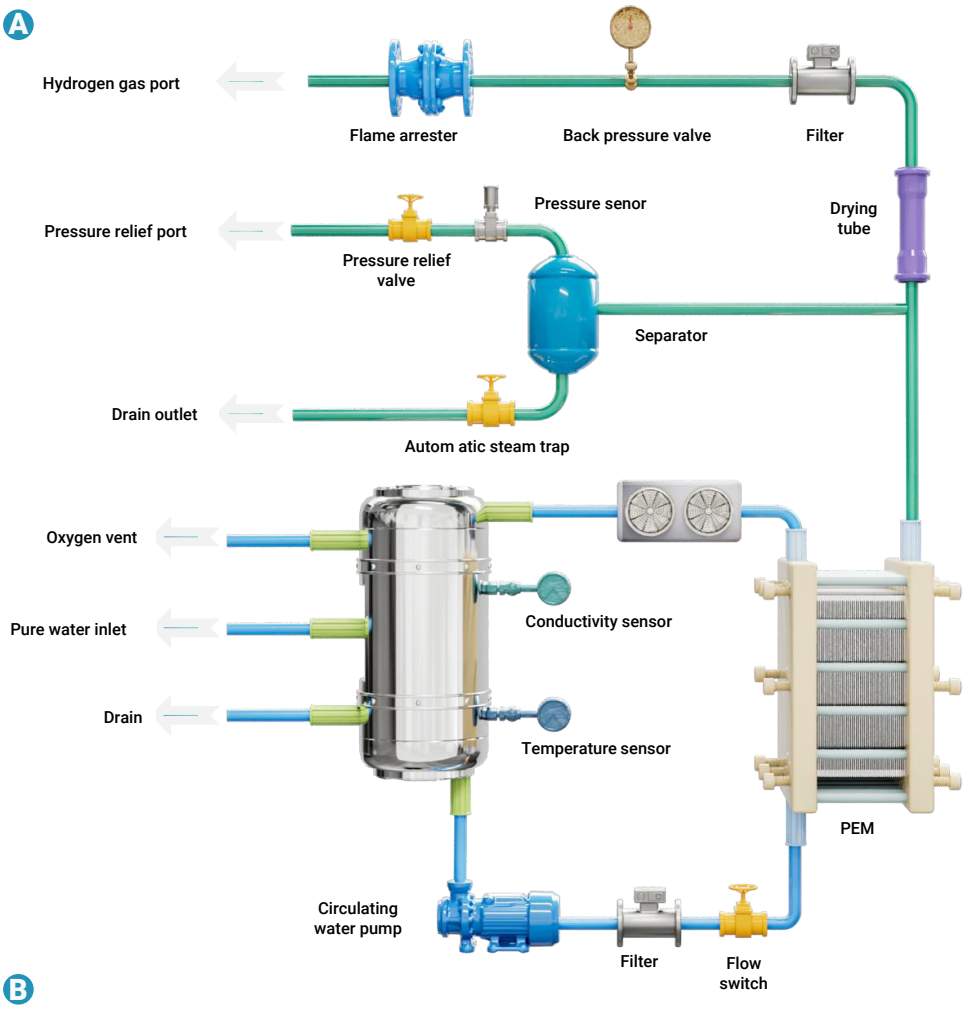

B

Parameters	Value
Rated voltage	220VDC:50HZ
Rated power	600 W
Hydrogen output flow rate	0-2000 mL/min
Hydrogen output pressure	0-1.5 MPa
Hydrogen purity	99.99 %
Water quality requirement	Greater than 15MΩ·cm
Operating temperature	Less than 50 ℃
Ambient	0-55℃, Relative humidity less than 85 %
Weight	45 kg
Dimension	600*450*650 mm

Figure 1. (A) The principle of the experimental system. (B) Key technical parameters and requirements of the PEM

Table 1. Key difference between cold and hot start-up

Aspect	Cold start-up	Hot start-up
Initial temperature	~10°C (ambient)	~30°C (preheated)
Membrane hydration	Low initial hydration; requires time for water redistribution	Near-equilibrium hydration state
Reaction kinetics	Slower kinetics due to low temperature; higher activation overpotential	Faster kinetics; lower initial overpotential
Thermal stress	Significant thermal shock if the current is applied directly	Reduced thermal gradient; milder stress
Start-up time	Longer (requires full temperature ramp from ambient)	Shorter (starts from elevated temperature)

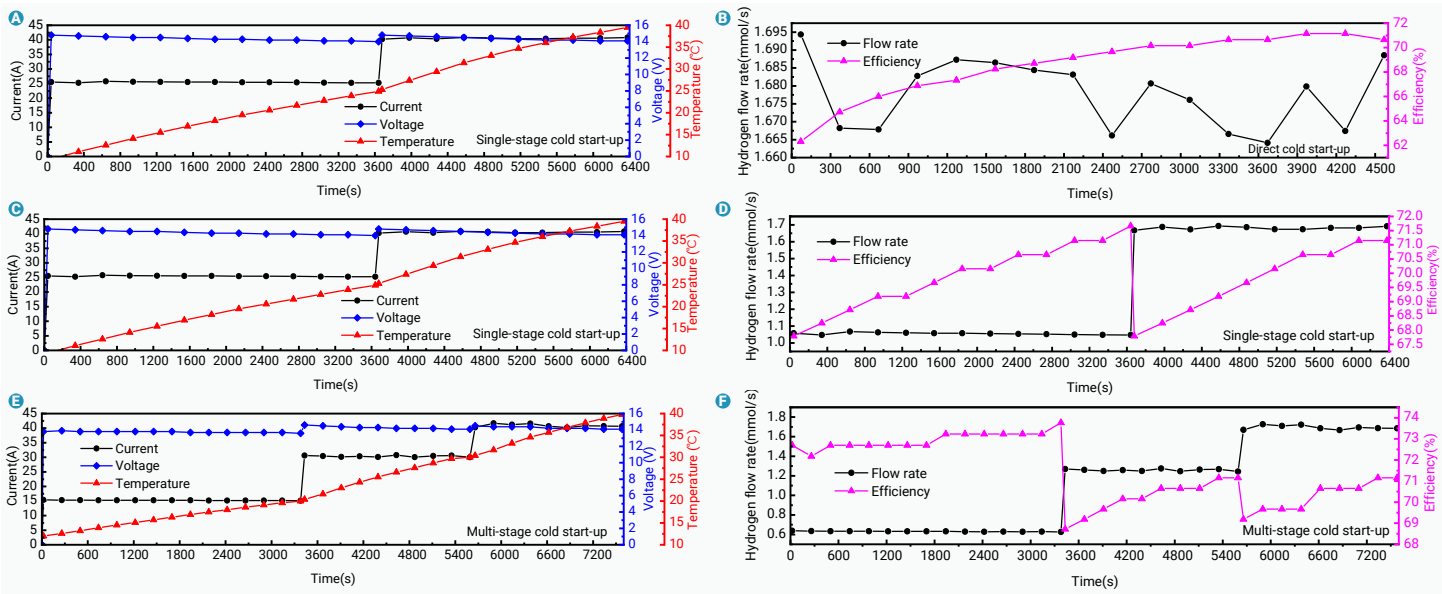

Figure 2. Cold start-up characteristics (A) Current, voltage, and temperature in DCS process (B) Hydrogen flow rate, and efficiency in DCS process (C) Current, voltage, and temperature in SCS process (D) Hydrogen flow rate, and efficiency in SCS process (E) Current, voltage, and temperature in MCS process (F) Hydrogen flow rate, and efficiency in MCS process

bance, including transient cell voltage response, temperature variation, gas production rate, and system efficiency.

Data analysis

The hydrogen production rate of the electrolyzer can be expressed as:

$$\dot{m}_{H2} = \eta_F N \frac{I}{2F} \tag{1}$$

where $\dot{m}_{H2}$ signifies the hydrogen production rate; η_F symbolizes the faradaic efficiency; N denotes the number of single electrolyzers; I indicates the electrolyzer current; F describes the faradaic constant; η_F is the faradaic efficiency.

The total hydrogen production can be expressed as:

$$m_{H2} = \int_0^t \dot{m}_{H2} dt \tag{2}$$

Average hydrogen production rate is defined as the total hydrogen production divided by the total start-up duration, characterizing the average hydrogen output capacity. It can be expressed as:

$$\overline{m}_{H2} = \frac{\int_{t_1}^{t_2} \dot{m}_{H2} dt}{t_2 - t_1} \tag{3}$$

The power of the PEM can be expressed as:

$$W = I \cdot V \tag{4}$$

The hydrogen production efficiency of the PEM can be expressed as:

$$\eta = \frac{m_{H2} Q_{LHVH2}}{W} \tag{5}$$

where Q_{LHVH2} is the lower heating value of hydrogen:

Average efficiency is defined as the integrated average of the ratio of total hydrogen energy to total electrical energy input over the start-up period, reflecting the comprehensive energy conversion efficiency during the start-up process.

$$\overline{\eta} = \frac{\int_0^t m_{H2} Q_{LHVH2} dt}{\int_i mits_0^t W dt} \tag{6}$$

To evaluate the smoothness of the PEM electrolyzer start-up process, the voltage rise rate is employed as a key dynamic indicator. This parameter quantifies the rate of voltage change over time during start-up. Its core significance lies in balancing start-up speed with material durability, thereby ensuring efficient, stable, and long-term operation of the electrolyzer. It can be expressed as:

$$\Delta V = \frac{V_{max} - V_0}{\Delta t} \tag{7}$$

where V_{max} indicates the peak start-up voltage; V_0 denotes the start-up initial voltage; Δt describes the total start-up time.

All three indicators are calculated using unified definitions and a global integration baseline, with data from all stages processed within the same time window in multi-step strategies, thus methodologically ensuring consistency and comparability between direct and multi-step start-up strategies.

RESULTS

Cold start-up characteristics of the system

The current-temperature setpoints are designed based on the low ionic conductivity of the membrane at low temperatures, using a stepwise current loading profile to avoid thermal stress and membrane degradation. Pre-experimental tests show that below 10°C, currents exceeding 20 A trigger voltage overshoot; at 20°C, 30 A significantly increases the heating rate; and at 30°C, 40 A causes no anomalies. This design balances start-up speed, system stability, and membrane durability.

Figure 2 depicts the cold start-up behavior of the PEM electrolyzer. Figure 2A presents the dynamic responses of current, voltage, and temperature in DCS process. During initial start-up, the current rapidly rises from 0 A to the rated 40 A within 70 s and stabilizes, while voltage synchronously peaks at 16.1 V; after 70 s, voltage gradually declines to 14.2 V as temperature increases, attributed to reduced cell overpotential at higher temperatures. The electrolyzer temperature continuously rises from an initial 11.6°C, reaching the rated operating temperature of 40°C after 4570 s, with the rate of temperature rise decelerating as the system approaches thermal equilibrium. Figure 2B shows that system efficiency improves from 62.3% at 70 s to 70.6% by 4570 s during DCS process, while the hydrogen production rate exhibits considerable variability throughout this phase. The efficiency improvement is primarily attributed to the enhanced reaction kinetics and membrane conductivity resulting from the temperature rise, as well as the reduced mass transport losses due to stabilized two-phase flow.

Figure 2C shows the dynamic response of current, voltage, and temperature during the SCS process. From 0-41 s, the current increases linearly from 0 A to 25.53 A, while voltage rises correspondingly from 0 V to 14.8 V; after 41 s, the current remains stable at 25.53 A, and voltage gradually decreases to 14 V. Following a current step command at 3641 s, the system reaches the

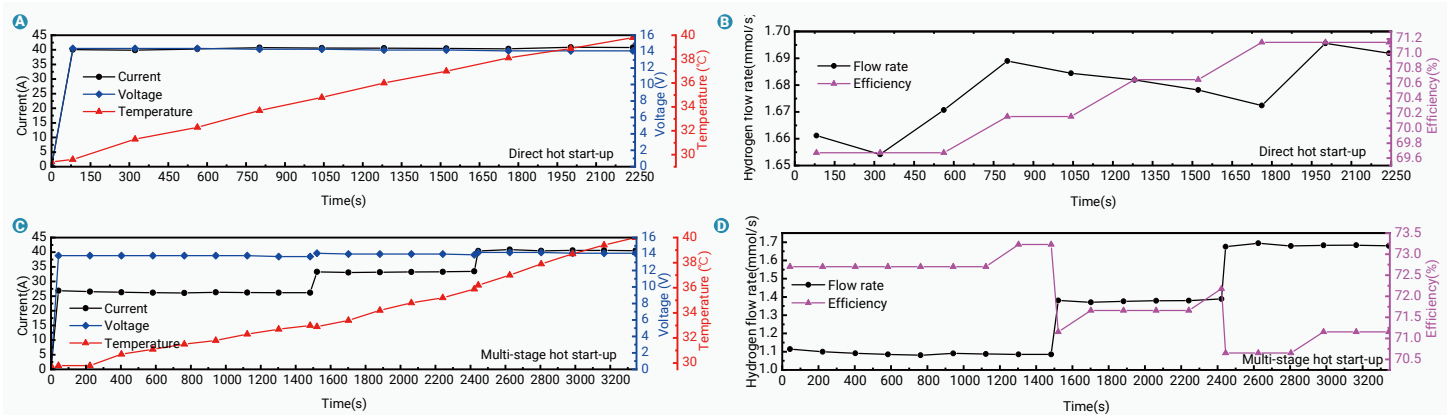

Figure 3. Hot start-up characteristics (A) Current, voltage, and temperature in DHS process (B) Hydrogen flow rate, and efficiency in DHS process (C) Current, voltage, and temperature in MHS process (D) Hydrogen flow rate, and efficiency in MHS process

rated current of 40 A by 3678 s, with voltage synchronously rising from 14 V to 14.8 V; thereafter, current stabilizes at 40 A while voltage slowly declines to 14.1 V. The electrolyzer temperature increases continuously, with a slightly lower rate before 3641 s compared to the 3641-6378 s interval, primarily due to increased thermal load from the current step. Figure 2D illustrates the evolution of system efficiency and hydrogen production rate in SCS process. During 41–3641 s, efficiency improves by 3.87% due to rising temperature; the current step between 3641–3678 s causes an abrupt 3.77% efficiency drop. This drop is attributed to increased overpotentials from the abrupt current rise, thermal lag delaying temperature response, and gas accumulation increasing mass transport losses. Subsequently, efficiency gradually recovers to 71.15%. The hydrogen production rate remains relatively stable around 1.06 mmol/s and 1.67 mmol/s in the two operational phases, respectively.

Figure 2E presents the dynamic response of current, voltage, and temperature during this MCS. The current undergoes three successive step increases: from 0 A to 15 A, then to 30 A, and finally to the rated 40 A. Voltage varies correspondingly with each step. During 0-20 s, the current rapidly rises to 15.38 A while voltage synchronously increases to 13.8 V; before the second current step, current remains essentially stable while voltage slightly decreases by 0.2 V; after applying the second step command at 3380 s, current reaches 30.62 A by 3431 s with voltage rising to 14.6 V; subsequently voltage decreases to 14.1 V. Following the final step at 5591 s, the system undergoes a 69 s dynamic process, reaching 40.27 A at 5660 s with voltage increasing to 14.5 V, after which current stabilizes at the rated value while voltage gradually declines to the rated 14.1 V. Throughout the three phases, temperature rises continuously, with each successive step exhibiting a higher rate of temperature rise than the preceding phase. Figure 2F illustrates the dynamic characteristics of hydrogen production rate and system efficiency in MCS process. Except during brief transient periods of current step changes, the hydrogen production rate remains relatively stable overall. System efficiency stays within its highest range (72.7%-73.8%) between the first and second current steps; after the second current increase, efficiency decreases to 68.7%-71.2% before the third step, and gradually recovers from 69.2% to 71.2% after completing the third step. The multi-step cold start-up strategy employs a stepwise current increase. This avoids thermal shock and allows gradual thermal equilibration of the membrane electrode assembly. It also facilitates proper hydration of the membrane. Consequently, reaction kinetics and two-phase mass transport are optimized. As a result, system stability and energy efficiency are significantly enhanced.

.

Hot start-up characteristics of the system

Figure 3A illustrates the dynamic profiles of current, voltage, and temperature during DHS process. Within 82 s, the current rapidly increases from 0 A to 40.07 A, while the voltage rises correspondingly from 0 V to 14.4 V. After 82 s, the current remains stable. However, due to the continuous temperature increase during the start-up process, the voltage gradually decreases and eventually stabilizes at 14.1 V. During this period, the temperature of the PEM electrolyzer increases from 29.4 °C to 39.8 °C within only 2,242 s. Figure 3B illustrates the DHS process dynamic characteristics of the hydrogen production rate and system efficiency during this process. It can be observed that as the temperature increases, the system efficiency continuously improves, rising from 69.67% to 71.15%. Due to the relatively short start-up time, the hydrogen production rate exhibits considerable fluctuation.

Figure 3C illustrates the MHS process dynamic characteristics of the PEM electrolyzer under dual current step conditions, including the dynamic response of current, voltage, and temperature. During start-up, the current increases in three discrete steps: from 0 A to 26 A, then to 33 A, and finally to 40 A. During the first step, the voltage rises from 0 V to 13.8 V and then slightly drops to 13.7 V. In the second, it increases from 13.7 V to 14.1 V before declining to 13.9 V. In the final phase, the voltage climbs from 13.9 V to 14.2 V and eventually stabilizes at the rated voltage of 14.1 V. Across these three steps, the temperature rise rate of the PEM electrolyzer accelerates correspondingly as the current progressively increases. Figure 3D illustrates the MHS process dynamic characteristics of the hydrogen production rate and system efficiency. Owing to the relatively small temperature fluctuations across the three stages, the hydrogen production rate remains comparatively stable in each phase. Due to the limited temperature variation, the efficiency of the PEM electrolyzer generally shows a positive correlation with the current and gradually decreases as the start-up proceeds.

These observations highlight the trade-off between start-up speed and system stability in hot start operations, consistent with the design rationale of the multi-step strategy aiming for improving energy efficiency and thermal management.

Step response characteristics of the PEM electrolyzer system

Figure 4 illustrates the dynamic response characteristics of the system under a direct load increase (DLI) process. Figure 4A shows that the initial system current was 25 A. After applying a step signal to a target current of 40 A at 0 s, the current increased to 40.3 A within 50 s, while the voltage rose from an initial value of 13.7 V to 14.2 V. Once the current reached the preset value, both current and voltage stabilized. Meanwhile, the system temperature continued to rise throughout the process, increasing from 33.6 °C to 34.8 °C. As shown in Figure 4B, during the DLI process, the hydrogen production rate increased steadily from an initial 1.062 mmol/s to 1.67 mmol/s, while the system efficiency decreased from 73.23% to 70.15% due to the increase in current. After the current stabilized, both the hydrogen production rate and system efficiency remained steady.

Figure 4C&D present the dynamic characteristics of the system as the current underwent a series of preset step changes, increasing successively from 25 A to 30 A, 35 A, and finally to 40 A. To ensure PEM stability, an 80 s interval was maintained after each current step before executing the next step. The first step occurred between 0 s and 20 s, during which the current increased from 25.25 A to 30.9 A, and the voltage rose correspondingly from 13.6 V to 13.9 V. The second step took place from 110s to 140 s, with the current rising from 30.6 A to 35.46 A and the voltage synchronously increasing from 13.9 V to 14.1 V. The final step was observed between 240 s and

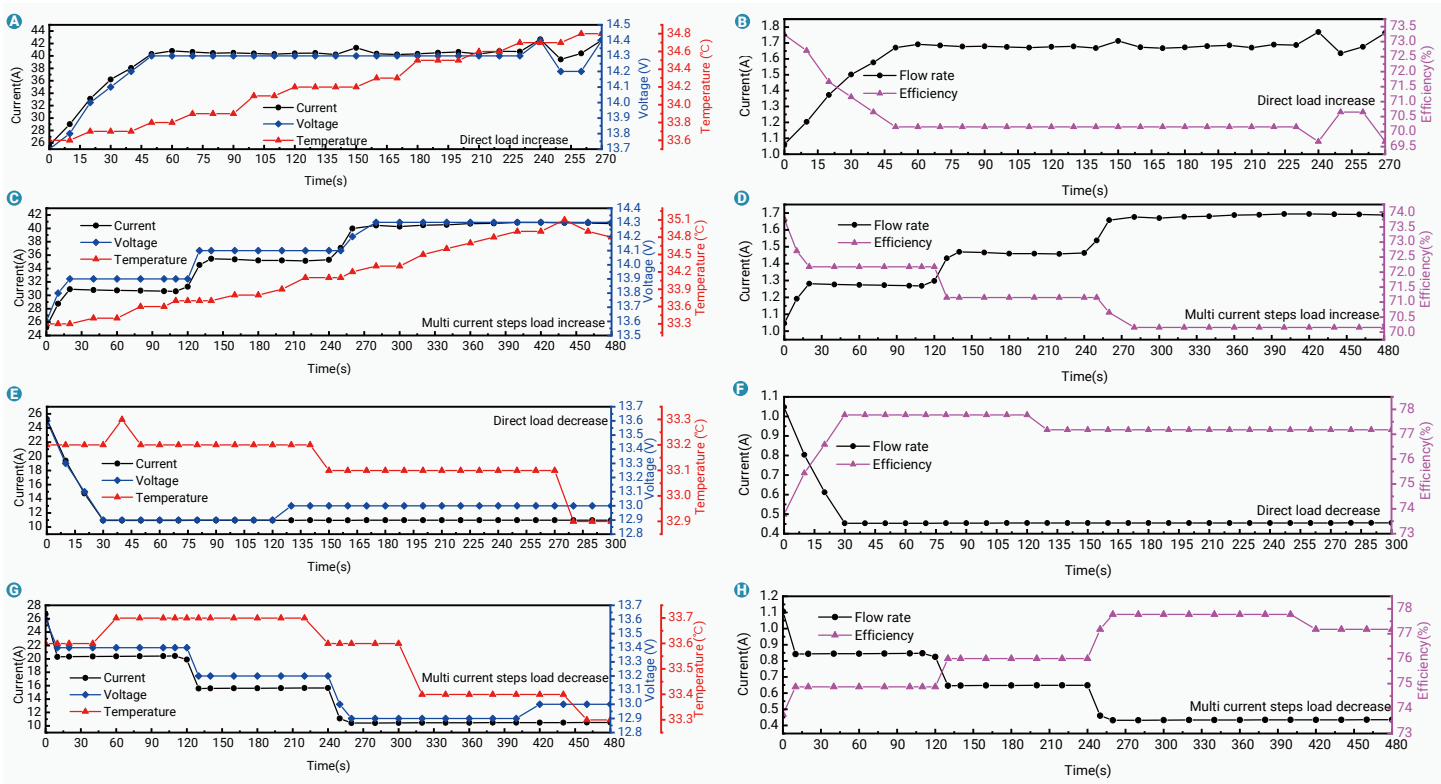

Figure 4. Load regulation Characteristics (A) Current, voltage, and temperature in DLI process (B) Hydrogen flow rate, and efficiency in DLI process (C) Current, voltage, and temperature in MLI process (D) Hydrogen flow rate, and efficiency in MLI process (E) Current, voltage, and temperature in DLD process (F) Hydrogen flow rate, and efficiency in DLD process (G) Current, voltage, and temperature in MLD process (H) Hydrogen flow rate, and efficiency in MLD process

260 s, where the current rose from 35.3 A to 39.97 A, and the voltage increased correspondingly from 14.1 V to 14.3 V. Throughout the entire process, the temperature continued to increase, rising from an initial 33.3 °C to 34.8 °C. As shown in Figure 4D, due to the minimal temperature variation during the process, the hydrogen production rate closely follows the trend of the current, exhibiting a stepwise increase across three successive stages. In contrast, the system efficiency shows an opposite trend to the current, which is attributed to increased polarization losses at higher currents.

Figure 4E&F illustrates the dynamic characteristics of the system as the current is reduced from 25 A to 10 A. At 0 s, the initial current of the PEM electrolyzer was 25.27 A. Following a command to reduce the current to 10 A, the current decreased to 10.94 A by 30 s, while the voltage correspondingly dropped from its initial value of 13.6 V to 13.1 V. The PEM temperature decreased continuously, falling from an initial 33.2 °C to 32.9 °C. This decline is attributed to the low current being insufficient to maintain the elevated operating temperature. As can be observed from Figure 4F, the abrupt drop-in hydrogen production rate was caused by the sudden decrease in current. Meanwhile, the system efficiency exhibited a trend of first rising and then falling, which is attributed respectively to the reduction in current and the subsequent decline in temperature. Notably, the temperature evolution during load increase and decrease exhibits distinct characteristics. During load increase, the heat input exceeds dissipation, leading to a continuous temperature rise. During load decrease, thermal inertia causes the temperature to initially stabilize and then decline gradually; under multi-step load reduction, thermal equilibrium is established at each constant-current stage, resulting in a step-like plateau, a pattern further amplified by measurement lag.

Figure 4G&H present the dynamic characteristics of the system as the current underwent a series of preset step decreases from 25 A to 20 A, 15 A, and finally to 10 A. To ensure PEM stability, an 80 s interval was maintained after each current step before proceeding to the next. The first step occurred between 0 s and 20 s, during which the current decreased from 26.67 A to 20.34 A, and the voltage dropped correspondingly from 13.6 V to 13.4 V. The second step took place from 110 s to 130 s, with the current declining from 20.43 A to 15.58 A and the voltage decreasing synchronously from 13.4 V to 13.2 V. The final step was observed between 240 s and 260 s, where the current fell from 15.65 A to 10.42 A, and the voltage decreased accordingly from 13.2 V to 12.9 V. Throughout the process, the temperature showed a continuous downward trend, decreasing from an initial 33.6 °C to a final 33.3 °C. As shown in Figure 4H, due to the minimal temperature variation, the hydrogen production rate closely follows the trend of the current, exhibiting a stepwise decrease across three successive stages. In contrast, the system efficiency initially increased owing to reduced polarization losses as the current decreased, and then declined slightly afterward due to the temperature drop. This trend reflects the combined effects of lowered polarization and altered electrochemical equilibrium under cooling conditions.

Comparison of start-up and load regulation methods

The comprehensive comparison of the three cold start-up schemes is shown in Figure 5A. Regarding the total start-up duration, the DCS is the shortest at 4570 s, followed by the SCS at 6378 s, with the MCS being the longest at 7580 s. However, in terms of start-up stability, the conclusion is reversed: the DCS exhibits the highest voltage rise rate of 3.52 mV/s; the SCS is 2.32 mV/s; and the MCS shows the lowest rate of 1.93 mV/s, indicating the most stable process. In terms of energy efficiency, the MCS achieves the highest average efficiency of 71.39%, outperforming the SCS 69.68% and the DCS at 68.47%. As for the hydrogen production rate, the constant current scheme ranks highest at 1.68 mmol/s, followed by the SCS at 1.32 mmol/s, and the MCS at 1.09 mmol/s. In summary, the MCS demonstrates optimal performance in stability and energy efficiency, making it suitable for high-reliability scenarios, while the DCS holds distinct advantages in applications requiring rapid start-up and immediate hydrogen production.

The comparison of the two hot start-up methods is shown in Figure 5B The DHS takes 2242 s with a voltage rise rate of 6.4 mV/s, while the MHS requires a longer duration of 3345 s and exhibits a lower voltage rise rate of 4.2 mV/s. The DHS achieves an average efficiency of 70.33%, which is 1.59% lower than that of the MHS. However, its average hydrogen production rate is higher at 1.62 mmol/s, exceeding the MHS by 2.99 mmol/s. In summary, the DHS offers advantages in start-up speed and hydrogen production rate,

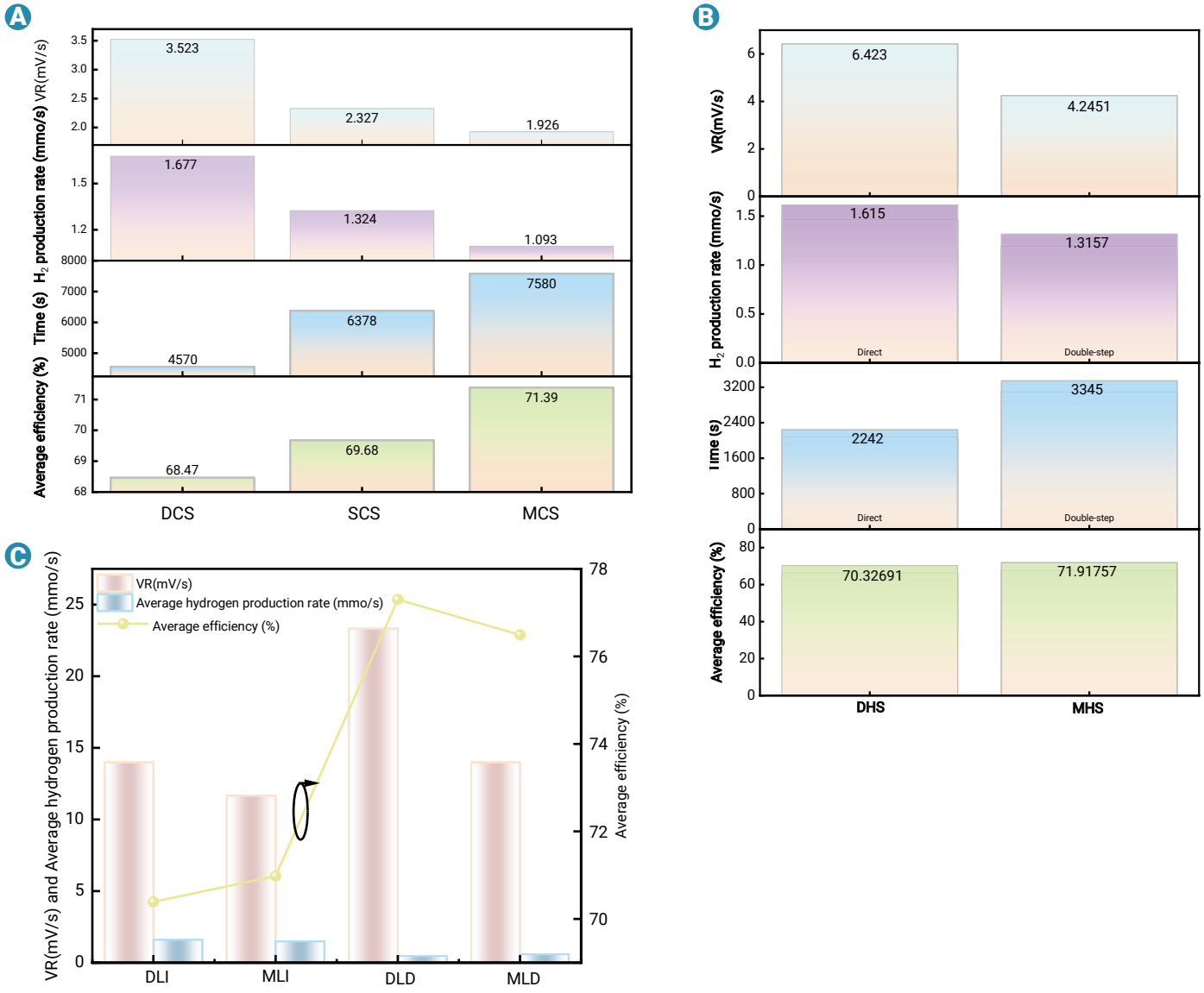

Figure 5. Integrated start-up and load regulation characteristics (A) cold start-up (B) hot start-up (C) load increase and decrease

whereas the MHS achieves higher energy efficiency but with a slower dynamic response. Practical system design requires a trade-off based on specific demands for time, efficiency, or hydrogen output.

The key performance indicators of the two current step-up/step-down schemes are compared in Figure 5C. During the load increase process, the multi-current steps load increase (MLI) achieves an efficiency of 70.98%, higher than the 70.39% of the direct load increase (DLI), but its hydrogen production rate of 1.5 mmol/s is slightly lower than the DLI's 1.62 mmol/s. During the load decrease process, the direct load decrease (DLD) reaches an efficiency of 77.30%, surpassing the multi-current steps load decrease (MLD)'s 76.49%, but its hydrogen production rate of 0.49 mmol/s is lower than the MLD's 0.6 mmol/s. Furthermore, the voltage rise rates under the four load variation modes are quantified as follows: DLI at 14 mV/s, MLI at 11.7 mV/s, DLD at 23.3 mV/s, and MLD at 14 mV/s. The voltage rise rates under direct variation modes are consistently higher than those under their corresponding multi-current step modes. This indicates that the selection of a current regulation strategy involves a trade-off between efficiency and hydrogen production performance, depending on whether priority is given to energy efficiency or the hydrogen output rate in a given application.

Comparison of load regulation methods

To systematically evaluate the comprehensive performance of the PEM electrolyzers under cold start-up, hot start-up, and load regulation operating modes, this study selects voltage rise rate, average efficiency, and average hydrogen production as key evaluation indicators. To objectively quantify the relative importance of each indicator, the entropy weight method is employed to adaptively assign weights to the three aforementioned criteria. On this basis, TOPSIS[28] is applied to calculate the closeness to the ideal state for each start-up and regulation mode, enabling comparison of the advantages and disadvantages of different operating strategies and identification of optimization pathways. This analytical approach provides a theoretical foundation and decision-making support for enhancing the dynamic response performance and overall energy efficiency of the PEM electrolyzers. The mathematical model of the entropy weight method can be expressed as:

$$p_{ij} = \frac{x_{ij}}{\sum_{i=1}^{m} x_{ij}} \tag{8}$$

$$e_j = -\frac{1}{\ln m} \sum_{i=1}^{m} p_{ij} \ln p_{ij} \tag{9}$$

$$w_j = \frac{1 - e_j}{\sum_{k=1}^{n} (1 - e_k)} \tag{10}$$

where x_{ij} represents the raw value of the j evaluation indicator for the i operat-

ing strategy; p_{ij} denotes the normalized proportion of x_{ij} within the j indicator; e_j is the entropy of the j indicator; m is the number of operating strategies; w_j is the entropy weight assigned to the j indicator; n is the total number of evaluation indicators.

According to the TOPSIS method, the relative closeness to the ideal solution can be defined and calculated as follows: shown in Equation 11, where Sd^- and Sd^+ represent the distances from a given alternative to the negative and positive ideal solutions, respectively, and C* denotes the ideal closeness coefficient.

$$C^* = \frac{Sd^-}{Sd^+ + Sd^-} \tag{11}$$

Based on the aforementioned entropy weigh-TOPSIS comprehensive evaluation method, this study systematically assessed the dynamic performance of different start-up modes and load regulation strategies. The overall evaluation results are presented in Figure 6.

(1) In cold start mode, the SCS achieved the highest relative closeness coefficient (C=0.5900), outperforming the DCS (C=0.4597) and MCS (C=0.5403). This indicates that it strikes the optimal balance among voltage rise rate, average efficiency, and hydrogen production.

(2) For hot start-up mode, the MHS (C=0.6635) demonstrated significant superiority over the DHS (C=0.3365), highlighting its better dynamic response and energy efficiency maintenance capability.

(3) During load regulation, the multi-step strategy significantly outperformed the direct method in both MLI (C=0.7184) and MLD (C=0.9804) scenarios. Its performance approached the ideal state, particularly during load decrease, suggesting that stepwise regulation can effectively mitigate voltage fluctuations and enhance overall system efficiency and hydrogen production stability.

In conclusion, stepwise strategies generally exhibit superior comprehensive performance during dynamic operation. This provides clear engineering guidance for optimizing the dynamic control strategies of PEM electrolyzers.

Key comparison between this study and other research

Compared with existing studies, previous research has largely focused on individual start-up modes or steady-state performance optimization, lacking systematic experimental comparisons across multiple dynamic operating conditions such as cold start-up, hot start-up, and load regulation (see Table 2). In terms of evaluation methods, existing studies typically rely on single indicators without constructing a multi-indicator evaluation framework covering voltage ramp rate, efficiency, and hydrogen production rate. Moreover, the assignment of indicator weights in these studies is often subjective. This study systematically compares multi-mode start-up and load regulation strategies on a unified experimental platform and introduces the entropy weight-TOPSIS method to achieve objective quantitative evaluation of multiple indicators. The results demonstrate that multi-step control strategies outperform direct control methods in both start-up stability and load response, providing experimental evidence and quantitative decision-making support for the optimized operation of PEM electrolyzers in scenarios coupled with fluctuating renewable energy sources.

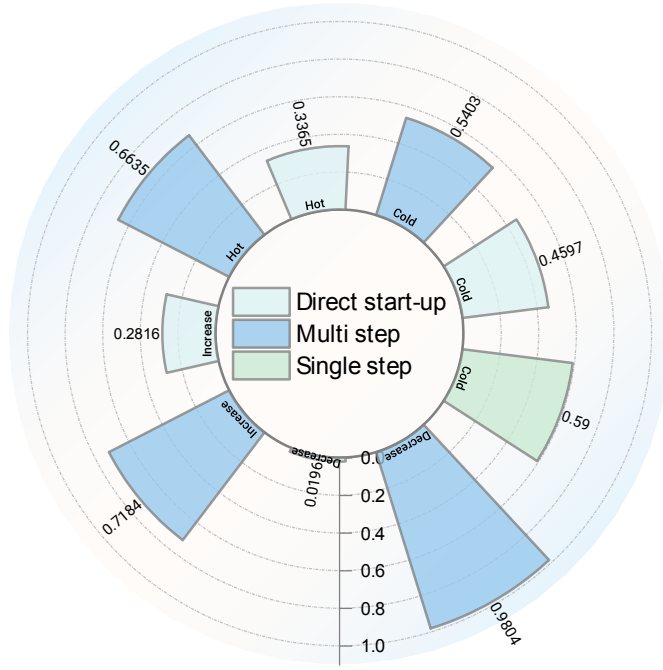

Figure 6. Comprehensive evaluation based on TOPSIS and entropy weight method

CONCLUSIONS

This study experimentally investigates the multi-mode performance of a PEM electrolyzer under cold start-up, hot start-up, and load regulation. Multiple control strategies were evaluated using an entropy-TOPSIS framework with indicators of voltage rise rate, average efficiency, and hydrogen production rate, providing methodological support and an experimental basis for optimizing dynamic operation strategies. The main conclusions are as follows:

(1) The cold start-up comparison reveals that, while the DCS achieves the fastest start-up, it exhibits the poorest stability. The MCS strategy offers the best stability and energy efficiency at the expense of the longest start-up time. The SCS strategy provides the most balanced performance, with a start-up time of 6378 seconds, a voltage rise rate of 2.32 mV/s, and an average efficiency of 69.68%, striking an optimal trade-off among start-up speed, system stability, and energy efficiency.

(2) The DHS strategy achieves a faster start-up time of 2242s and a higher average hydrogen production rate of 1.62 mmol/s, but exhibits a higher voltage rise rate of 6.4 mV/s and a lower average efficiency of 70.33%. In contrast, the MHS strategy, although requiring a longer start-up time of 3345 s and yielding a slightly lower hydrogen production rate of 1.32 mmol/s, demonstrates a lower voltage rise rate of 4.2 mV/s and a higher average efficiency of 71.92%, indicating superior system stability and energy efficiency.

(3) For load increase, DLI regulation achieves 1.62 mmol/s but 70.39% effi-

Table 2. Key comparison between this study and other research

Research	Research content	Key methods	Evaluation indicators	Contributions
This study	Cold start-up, hot start-up, load regulation	Multi-step/direct control, entropy weight-TOPSIS	Voltage ramp rate, average efficiency, average hydrogen production rate	Systematic comparison of multi-mode start-up and load Entropy weight-TOPSIS enables multi-indicator quantitative evaluation
Rauls et al. [22]	Start-up behavior	Electric heating, heat-up efficiency, and dimensionless heat-up number	Heat-up efficiency, heat-up time	Partial-load start-up achieves 74.0% heat-up efficiency
Keller et al. [26]	Dynamic demand response	Dynamic ramping constraints, short-term overload, and economic dispatch	Operating cost, model prediction error, overload capability	Short-term overload reduces operating cost by 3.8%
Kesercioglu et al. [27]	Performance optimization	Taguchi method, optimization of temperature, torque, flow rate	Hydrogen production rate, efficiency	Optimized steady-state conditions: 80°C, 10 Nm, 10 mL/min

Nomenclature

F	faraday constant (C/mol)
I	current (A)
m_{H2}	hydrogen quantity (mmol)
$\dot{m}_{H2}$	hydrogen flow rate (mmol/s)
$\overline{m}_{H2}$	average hydrogen flow rate (mmol/s)
N	the number of single electrolyzers
Q_{LHVH2}	the lower heating value of hydrogen (kJ)
t	time (s)
V	voltage (V)
W	The power of the PEM (kW)
Greek alphabet	
η_F	faraday efficiency (%)
η	hydrogen production efficiency (%)
$\overline{\eta}$	average hydrogen production efficiency (%)
Abbreviations	
DCS	Direct cold start-up
DHS	Direct hot start-up
DLI	Direct load increase
DLD	Direct load decrease
MCS	Multi-stage cold start-up
MHS	Multi-stage hot start-up
MLI	Multi-current steps load increase
MLD	Multi-current steps load decrease
SCS	Single-stage cold start-up

ciency and 14 mV/s voltage rise, while MLI regulation improves efficiency to 70.98% and reduces voltage rise to 11.7 mV/s with a slight drop in hydrogen production to 1.5 mmol/s. For load decrease, DLD regulation shows 77.30% efficiency but 23.3 mV/s voltage rise and 0.49 mmol/s hydrogen production, whereas MLD regulation reduces voltage rise to 14 mV/s and increases hydrogen production to 0.6 mmol/s while maintaining high efficiency. Overall, multi-step regulation offers better stability and comprehensive performance.

(4) The entropy weight-TOPSIS evaluation results demonstrate that stepwise control strategies outperform direct control strategies across all operating modes. Under cold-start conditions, the SCS achieves the highest relative closeness of 0.5900. For hot-start operation, the MHS attains a relative closeness of 0.6635, significantly higher than that of the DHS (0.3365). In load regulation, the multi-step strategy yields relative closeness values of 0.7184 and 0.9804 for load increase and load decrease, respectively, indicating a state closer to the ideal. These findings indicate that stepwise control strategies can effectively enhance the system's dynamic response and operational stability.

(5) The start-up and load regulation strategies in this study are applicable to different hydrogen production scenarios. SCS suits grid-connected operation, MHS is appropriate for off-grid operation, and multi-step load regulation is recommended for fluctuating power sources such as wind and photovoltaics. Multi-step regulation reduces voltage fluctuations and thermal stress, extending lifespan and lowering maintenance costs.

Future research can focus on start-up strategies tailored to different application scenarios, such as grid-connected hydrogen production, off-grid operation, warm restart, and coupling with fluctuating power sources.

REFERENCES

1. Xu Z.Y. and Wang R.Z. (2024). Prospects of heat pump for thermal energy decarbonization. *Innov. Energy* **1**:100032. DOI:10.59717/j.xinn-energy.2024.100032
2. Jiao F., Chen C., Liu T.X., et al. (2024). Insights of water-to-hydrogen conversion from thermodynamics. *Innov. Energy* **1**:100004. DOI:10.59717/j.xinn-energy.2024.100004
3. Lin B. and Li J. (2015). Analyzing cost of grid-connection of renewable energy development in China. *Renew. Sustain. Energy Rev.* **50**:1373–1382. DOI:10.1016/j.rser.2015.04.194
4. Luo D., Liu J., Wu H., et al. (2025). Advancing smart net-zero energy buildings with renewable energy and electrical energy storage. *J. Energy Storage* **114**:115850. DOI:10.1016/j.est.2025.115850
5. Ozarslan A. (2012). Large-scale hydrogen energy storage in salt caverns. *Int. J. Hydrogen Energy* **37**:14265–14277. DOI:10.1016/j.ijhydene.2012.07.111
6. Ferraren D. and Abundo M. (2021). A review of biohydrogen production technology for hydrogen fuel cells. *Renew. Sustain. Energy Rev.* **151**:111413. DOI:10.1016/j.rser.2021.111413
7. Luo L., Cristofari C. and Levrey S. (2023). Cogeneration systems and energy efficiency via exergy analysis. *J. Energy Storage* **66**:107433. DOI:10.1016/j.est.2023.107433
8. Handayani K., Anugrah P., Goembira F., et al. (2022). ASEAN pathways to net-zero emissions power sector in 2050. *Appl. Energy* **311**:118580. DOI:10.1016/j.apenergy.2022.118580
9. Ahn S.Y., Kim K.J., Kim B.J., et al. (2023). Trends of catalysts and sorbents for hydrogen production. *Renew. Sustain. Energy Rev.* **186**:113635. DOI:10.1016/j.rser.2021.113635
10. Tello A., Catano F.A., Arunachalam A., et al. (2025). Green hydrogen production by photovoltaic-assisted electrolysis. *Int. J. Hydrogen Energy* **107**:378–395. DOI:10.1016/j.ijhydene.2024.04.333
11. Zhang C., Wang J., Ren Z., et al. (2021). Wind-powered electrolyzer for hydrogen production. *Int. J. Hydrogen Energy* **46**:34550–34564. DOI:10.1016/j.ijhydene.2021.08.029
12. Olivier P., Bourasseau C. and Bouamama P.B. (2017). Low-temperature electrolysis system modelling. *Renew. Sustain. Energy Rev.* **78**:280–300. DOI:10.1016/j.rser.2017.03.099
13. Zhang J., Wang Z., He Y., et al. (2023). LCA comparison of wind hydrogen production systems. *Sustain. Energy Technol. Assess.* **60**:103515. DOI:10.1016/j.seta.2023.103515
14. Hirokazu K., Kensaku N., Naoto T., et al. (2023). Influence of renewable fluctuations on electrolysis. *Int. J. Hydrogen Energy* **48**:4572–4593. DOI:10.1016/j.ijhydene.2022.11.018
15. Sebbahi S., Assila A., Belghiti A.A., et al. (2024). Advances in alkaline water electrolysis. *Int. J. Hydrogen Energy* **82**:583–599. DOI:10.1016/j.ijhydene.2024.07.428
16. Zhang B., Harun N.F., Zhou N., et al. (2023). A real-time multiphysics model of a pressurized solid oxide electrolysis cell (SOEC) for cyber-physical simulation. *Energy Convers. Manage.* **298**:117778. DOI:10.1016/j.enconman.2023.117778
17. Ruuskanen V., Koponen J., Huoman K., et al. (2017). PEM water electrolyzer model for a power-hardware-in-loop simulator. *Int. J. Hydrogen Energy* **42**:10775–10784. DOI:10.1016/j.ijhydene.2017.03.046
18. Asiaban S., Bozalakov D. and Vandevelde L. (2024). Dynamic model of PEM electrolyser for integration into large-scale power systems. *Energy Convers. Manage. X* **23**:100610. DOI:10.1016/j.ecmx.2024.100610
19. Midilli A., Inac S. and Ozsaban M. (2017). Exergetic sustainability indicators for hydrogen systems. *Int. J. Hydrogen Energy* **42**:21379–21391. DOI:10.1016/j.ijhydene.2017.04.299
20. Ganjehsarabi H. (2019). Mixed refrigerant as working fluid in Organic Rankine Cycle for hydrogen production driven by geothermal energy. *Int. J. Hydrogen Energy* **44**:18703–18711. DOI:10.1016/j.ijhydene.2018.11.231
21. Corumlu V., Ozsoy A. and Ozturk M. (2018). Thermodynamic studies of a novel heat pipe evacuated tube solar collectors based integrated process for hydrogen production. *Int. J. Hydrogen Energy* **43**:1060–1070. DOI:10.1016/j.ijhydene.2017.10.107
22. Rauls E., Hehemann M., Keller R., et al. (2023). Favorable Start-Up behavior of polymer electrolyte membrane water electrolyzers. *Appl. Energy* **330**:120350. DOI:10.1016/j.apenergy.2022.120350
23. Sakas G., Rentschler P., Kosonen A., et al. (2025). Dynamic mass and energy balance model of a 50 kW proton exchange membrane electrolyzer system. *Appl. Energy* **382**:125199. DOI:10.1016/j.apenergy.2024.125199
24. Hüner B. (2024). Mathematical modeling of an integrated photovoltaic-assisted PEM water electrolyzer system for hydrogen production. *Int. J. Hydrogen Energy* **79**:594–608. DOI:10.1016/j.ijhydene.2024.07.041
25. Mraoui A., Benyoucef B. and Hassaine L. (2018). Experiment and simulation of electrolytic hydrogen production: Case study of photovoltaic-electrolyzer direct connection. *Int. J. Hydrogen Energy* **43**:3441–3450. DOI:10.1016/j.ijhydene.2017.11.035
26. Keller R., Baader F.J., Bardow A., et al. (2025). Experimental demonstration of dynamic demand response scheduling for PEM-electrolyzers. *Appl. Energy* **393**:126014. DOI:10.1016/j.apenergy.2025.126014
27. Kesercioglu M.A., Boyacı San F.G., Sözbir N., et al. (2025). Performance optimization of PEM electrolyzers: An experimental and Taguchi-based approach. *Int. J. Hydrogen*

Energy **152**:150214. DOI:10.1016/j.ijhydene.2025.150214
28. Wang Y. and Xie G. (2023). Multi-objective optimisation of K-shape notch multi-way spool valve using CFD analysis, discharge area parameter model, and NSGA-II algorithm. *Energy Convers. Manage.* **283**:116952. DOI:10.1016/j.enconman.2023.116952

FUNDING AND ACKNOWLEDGMENTS

This research was supported by the National Natural Science Foundation of China (Nos. 52276001, 52206217, and U22B20112) and Natural Science Foundation of Chongqing, China (New Chongqing Youth Innovation Talent Program, No. CSTB2025YITP-QCRCX0068). Academic Papers of the 28th Annual Meeting of the China Association for Science and Technology.

AUTHOR CONTRIBUTIONS

Hao Zhang Writing-review & editing, Writing-original draft, Visualization, Validation, Data curation, Investigation, Formal analysis, Conceptualization. Pengyun Wang Investigation, Formal analysis, Data curation. Lin Zhao Writing-original draft, Visualization . Qibin Li Methodology, Conceptualization, Funding acquisition. Haoshui Yu Writing-review & editing, Validation. Tao Yang Methodology, Conceptualization, Funding acquisition. Jun Shen Funding acquisition. All authors contributed to and approved the final version of the manuscript.

DECLARATION OF INTERESTS

Jun Shen is an Editorial Board member of The Innovation Energy and was blinded from reviewing or making final decisions on the manuscript. Peer review was handled independently of this member and their research group. The other authors declare no conflicts of interest.

DATA AND CODE AVAILABILITY

The data that support the findings of this work are available from the corresponding author upon reasonable request.